



Synthesis and luminescent properties of gadolinium aluminates phosphors

Marcela G. Matos, Paulo S. Calefi, Katia J. Ciuffi, Eduardo J. Nassar*

Universidade de Franca, Av. Dr. Armando Salles Oliveira, 201, CEP 14404-600, Franca, SP, Brazil

ARTICLE INFO

Article history:

Received 9 December 2010
Received in revised form 6 April 2011
Accepted 15 April 2011
Available online 30 April 2011

Keywords:

Europium III
Sol–gel process
Optical properties
Luminescence

ABSTRACT

In this work, aluminum–gadolinium oxides with different phases were prepared by the non-hydrolytic sol–gel route, using lower temperatures than those employed in methods such as solid-state reaction and Pechini method. The influence of heating treatment on sample structure was investigated. The formation process and the local structure of the samples are discussed on the basis of thermal, X-ray diffraction, photoluminescence (PL) spectroscopy, and infrared spectroscopy analyses. The quantum efficiency of Eu^{3+} in the different phases obtained in this studied was evaluated. Initial crystallization and the GdAlO_3 phase were observed at temperatures around 400 °C. PL data of all the samples revealed the characteristic transition bands arising from the $^5\text{D}_0 \rightarrow ^5\text{F}_j$ ($j = 0, 1, 2, 3, \text{ and } 4$) manifolds under maximum excitation at 275, 393, and 467 nm in all cases. The $^5\text{D}_0 \rightarrow ^7\text{F}_2$ transition often dominates the emission spectra, indicating that the Eu^{3+} ion occupies a site without inversion center.

© 2011 Elsevier B.V. All rights reserved.

1. Introduction

Materials that emit in the UV–Vis range after absorption of high-energy photons are known as scintillators. Based on this property, these materials provide a myriad of applications as radiation detectors in the areas of medical diagnostic imaging, industrial inspection, dosimetry, and nuclear medicine [1]. Several research activities related to the preparation and characterization of lanthanides-doped phosphors for use solid-state lasers, color TV monitors, and fluorescent lamps have been reported [2]. Materials with specific optical and structural properties are required for different utilizations. In general, no phosphor completely fulfills the requirements of all applications. Thus, improvements in one or more properties are desirable in the quest for efficient X-ray phosphors, which must have properties that include high density, chemical stability, radiation hardness, high luminescent yield and, in some cases, short lifetime. Moreover, phosphors must be inexpensive and easily obtained [3]. Information on the properties of these materials, such as thermal expansion coefficient, specific heat, and thermal conductivity, as a function of temperature is essential to evaluate the effect of temperature on their thermophysical properties under temperature gradients [4]. Gadolinium aluminate is currently being researched as candidate material for neutron absorption [4,5], and it is a promising candidate for optical, magnetic, electronic, and structural applications [6]. Combinations of Gd_2O_3 – Al_2O_3 systems, such as GdAlO_3 (GAP), $\text{Gd}_3\text{Al}_5\text{O}_{12}$ (GAG),

and $\text{Gd}_4\text{Al}_2\text{O}_9$ (GAM) are chemically stable compounds that are suitable hosts for replacement with lanthanides ion ($\text{Ln}^{3+} = \text{Ce}, \text{Nd}, \text{Er}, \text{Eu}, \text{Tb}, \text{Sm}, \text{ and } \text{Dy}$) [7]. From a structural viewpoint, perovskite-type oxides (GdAlO_3) score over fluoride-based oxide systems. The former oxides offer two sites (Gd and Al) for aliovalent doping, thereby creating vacancies in the oxygen sublattice and aiding migration of oxygen ions through the lattice [8]. Among these compounds, gadolinium aluminum perovskite (GAP) is an important phosphor host material with perovskite structure [9]. GAP is normally synthesized at high temperatures by a solid-state reaction between aluminum and gadolinium oxides. Such conditions result in several problems concerning particle size, impurity, and formation of other phases [10]. The non-hydrolytic sol–gel route, on the other hand, involves the reaction of a metal halide with an oxygen donor such as ether, alcohol, or another donor under non-aqueous conditions, to form an inorganic oxide [11]. The direct advantages of this technology include the production of novel chemical compositions with unique properties, easy stoichiometric control, good homogeneity through mixture of the starting materials at the molecular level in solution, relatively low reaction temperature, shorter heating time, less potential for cross-contamination, small size and narrow particle size distribution, excellent purity, and more convenient preparation routes that minimize sample manipulation [12–28].

In this work, the influence of the heat treatment on the preparation of the $\text{Gd}(\text{Eu})\text{Al}$ oxide powder using a non-hydrolytic sol–gel method was investigated. The powder was dried and treated at 100, 400, 600, 800, and 1000 °C for 4 h and structurally characterized by thermal analysis (TG/DTA), X-ray diffraction (XRD), photoluminescence (PL), and infrared spectroscopy (IR).

* Corresponding author. Tel.: +55 16 37118871; fax: +55 16 37213266.

E-mail addresses: mgmtos@yahoo.com.br (M.G. Matos), ejnassar@unifran.br (E.J. Nassar).

2. Experimental

2.1. Preparation of solution of lanthanides ion chloride (LnCl_3) $1 \times 10^{-1} \text{ mol L}^{-1}$ ($\text{Ln} = \text{Eu}^{3+}$ and Gd^{3+})

The lanthanides oxides were calcined at 900°C for 2 h. Then, 0.9100 g Gd_2O_3 or 0.8798 g Eu_2O_3 was dissolved in H_2O and HCl 6 mol L^{-1} . Excess HCl and H_2O were evaporated. The ethanol was then added and evaporated three times. The final concentration of Ln ion in the ethanolic solution was $1.0 \times 10^{-1} \text{ mol L}^{-1}$.

2.2. AlCl_3

Anhydrous aluminum chloride was purchased from Vetec®.

2.3. Sol–gel synthesis of the Gd–Al host

The preparation of the gel was carried out in oven-dried glassware. The material was synthesized by the non-hydrolytic method described by us [10,24,29,30], via modification of the method described by Acosta et al. [31]. One gram of AlCl_3 and 20 mL ethanol (EtOH) were reacted with 2.5 mL EuCl_3 solution and 22.5 mL GdCl_3 solution (prepared as described in Section 2.1). The mixture was kept under reflux (the condenser was placed in a thermostatic bath at -5°C) for 4 h in silicon bath, at 110°C and under argon atmosphere. After reflux, the mixture was cooled and aged overnight in the mother liquor at room temperature (RT), because precipitation continues through aging in the mother liquor. The solvent was then removed under vacuum. The powders were dried and received heat treatment at 100, 400, 600, 800, and 1000°C for 4 h in air. The lanthanide ion dopant (Eu^{3+}) was added at a molar ratio of 1% in relation to the Gd^{3+} ion.

2.4. Characterization techniques

Thermal analysis (TG/DTG/DTA) was carried out (Thermal Analyst 2100 – TA Instruments SDT 2960 simultaneous DTA–TG) in nitrogen atmosphere at a heating rate of $20^\circ\text{C}/\text{min}$, from 25 to 1000°C .

The X-ray diffraction (XRD) measurements were performed at room temperature using a Rigaku Geigerflex D/max-c diffractometer with monochromated $\text{Cu K}\alpha$ radiation ($\lambda = 1.54 \text{ \AA}$). Diffractograms were recorded in the 2θ range from 4° to 80° at a resolution of 0.05° .

Photoluminescence (PL) data were obtained under continuous Xe lamp (450 W) excitation with a spectrofluorometer (SPEX – Fluorolog II) at room temperature. The emission was collected at 90°C from the excitation beam. The slits were placed at 1.0 and 0.2 mm for excitation and emission, respectively, giving a bandwidth of 3.5 and 0.5 nm. Oriol 58916 (exc.) and Corning 97612 (em.) filters were used.

The infrared absorption spectra (FTIR) were acquired on a Perkin-Elmer 1739 spectrophotometer with Fourier transform, using the KBr pellet technique, with a sample/KBr ratio of 1:300, approximately.

3. Results and discussion

3.1. Thermal analysis (TG/DTG/DTA)

Fig. 1 shows the TG/DTG/DTA curves obtained for the precursors of the Gd(Eu)–Al–O samples prepared by the non-hydrolytic method and dried at 50°C .

The TG/DTG/DTA curves reveal peaks accompanied by mass losses at 70, 120, 170, and 270°C , attributed to the loss of water

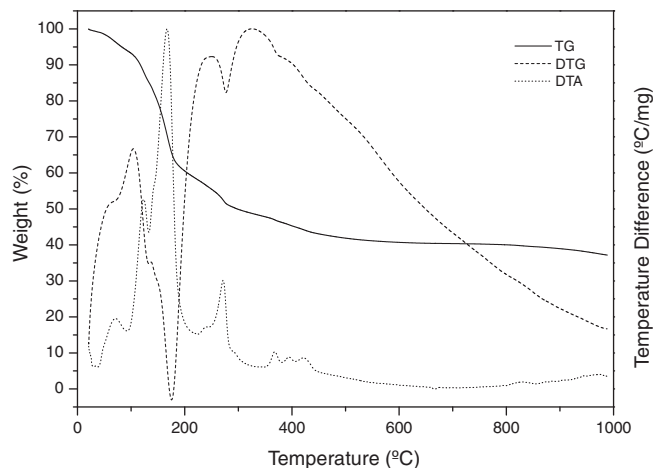


Fig. 1. TG/DTG/DTA curves for the precursors of the Gd(Eu)–Al–O samples dried at 50°C .

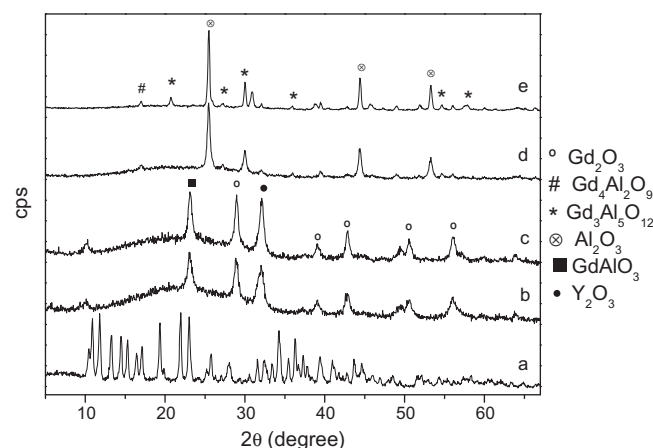


Fig. 2. X-ray diffraction patterns of the Gd(Eu)–Al–O precursor gels treated at (a) 100, (b) 400, (c) 600, (d) 800, and (e) 1000°C for 4 h.

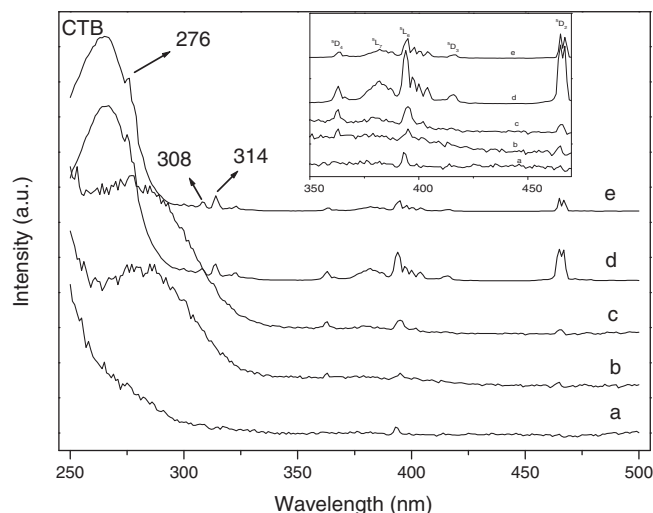


Fig. 3. Excitation spectra of the Eu^{3+} ion in the Gd(Eu)–Al–O host treated at (a) 100, (b) 400, (c) 600, (d) 800, and (e) 1000°C for 4 h, $\lambda_{\text{em}} = 616 \text{ nm}$.

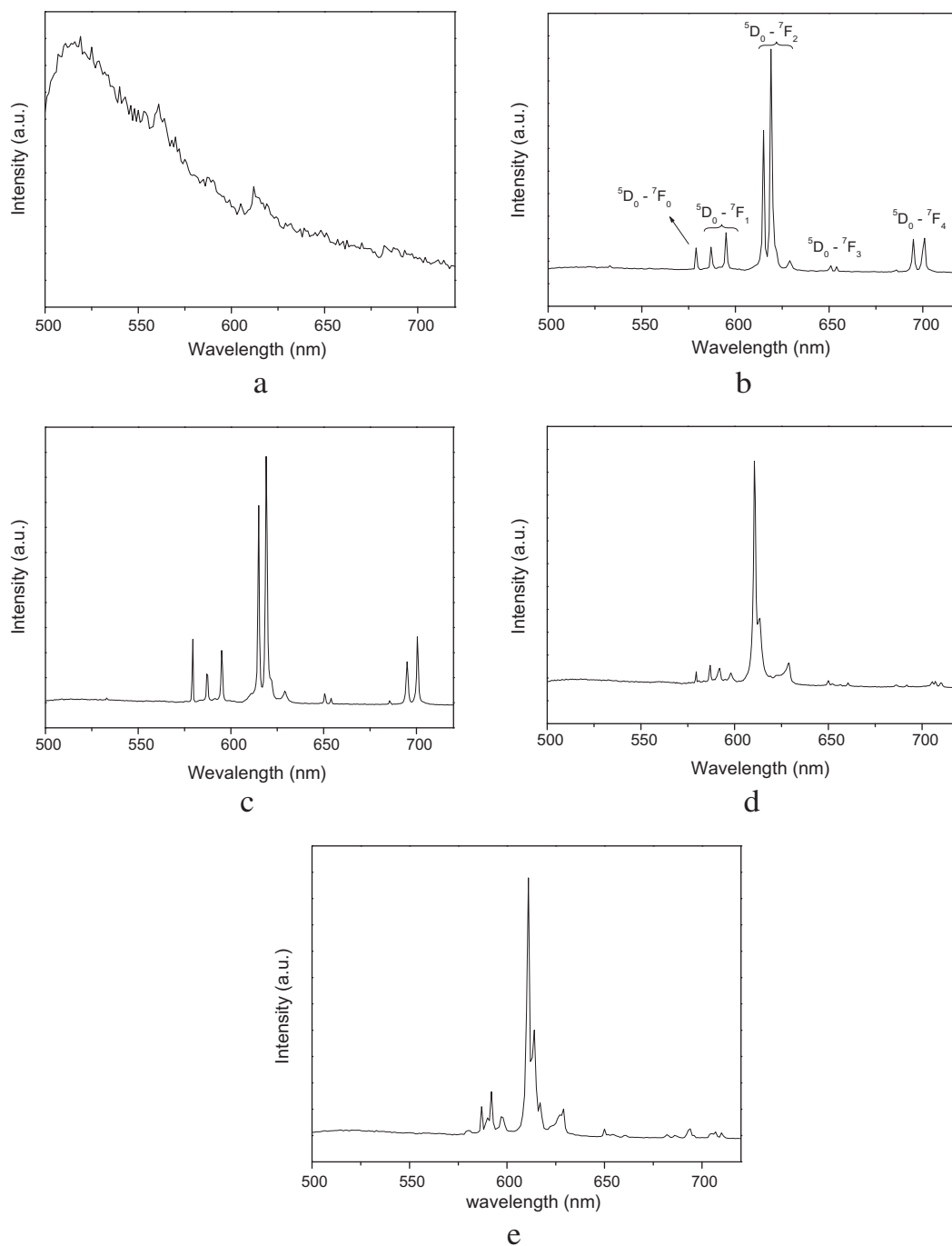


Fig. 4. Emission spectra of the Eu^{3+} ion in the $\text{Gd}(\text{Eu})\text{-Al-O}$ samples treated at (a) 100, (b) 400, (c) 600, (d) 800, and (e) 1000 °C for 4 h, excited at CTB.

molecules weakly bound to the oxide and solvent molecules. Another mass loss appears at 400 °C, ascribed to pyrolysis of organic matter remaining from the synthesis.

The DTA curve displays small exothermic peaks around 400 and 970 °C, due to phase transition. The exothermic peak around 400 °C can be due to crystallization of different phases, as observed in the XRD patterns. The crystallization temperature of the sample obtained by the non-hydrolytic route is low compared with those of materials obtained by Cizauskaite et al. (1000 °C) and by other methods such as Pechini (850 °C) and solid-state reactions (1450 °C) [3,4,6]. The other peak at approximately 970 °C is characteristic of a second crystallization, as can be seen from the formation of different phases in the XRD patterns.

The thermogravimetric analysis shows that most of the weight loss, around 40% (w/w), is associated with the loss of water and weakly bound solvent molecules in the sample, which takes place mainly between 70 and 250 °C.

3.2. X-ray diffraction (XRD)

Fig. 2 presents the XRD patterns of the powders obtained after treatment at 100, 400, 600, 800, and 1000 °C for 4 h.

The XRD pattern of the precursor powder of $\text{Gd}(\text{Eu})\text{-Al-O}$ prepared by the non-hydrolytic sol-gel process and dried at 100 °C reveals the presence of several peaks that can be due to a mixture of the precursors in the sample (Fig. 2). Crystallization of

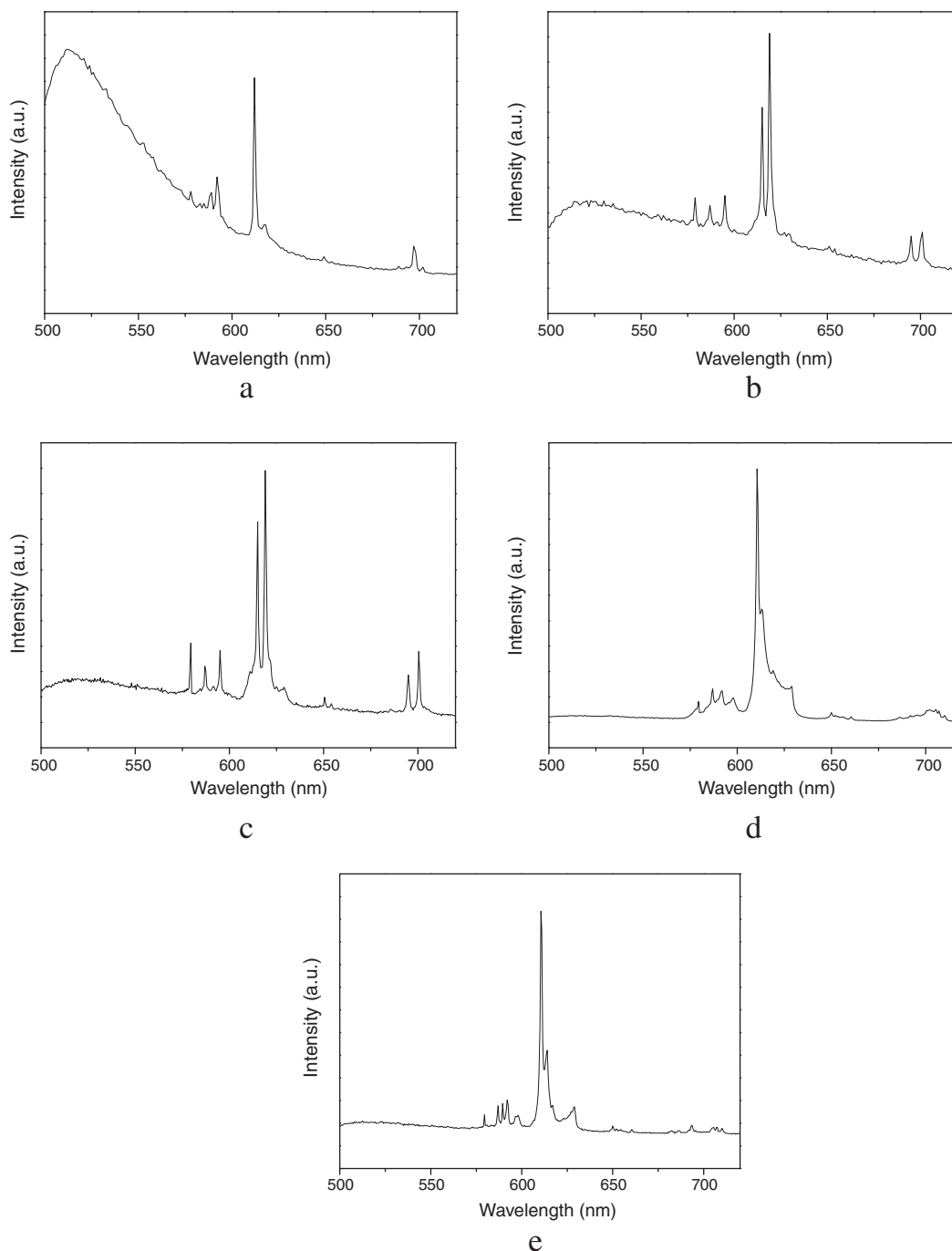


Fig. 5. Emission spectra of the Eu^{3+} ion in the $\text{Gd}(\text{Eu})\text{-Al-O}$ samples treated at (a) 100, (b) 400, (c) 600, (d) 800, and (e) 1000 °C for 4 h, excited at 393 nm (${}^5\text{L}_6$ level).

the materials becomes evident with increasing temperatures of heat treatment. An amorphous phase appears in the case of the powders treated at 400, 600, and 800 °C, but the amount of this phase decreases with increasing temperature. The onset of crystallization is observed at 400 °C. Several phases can be observed for the samples treated at 400 and 600 °C, such as GdOCl (JCPDF No. 12-718), EuOCl (JCPDF No. 12-163), Gd_2O_3 (JCPDF No. 43-1014), Eu_2O_3 (JCPDF No. 12-393), and the oxide mixture of Gd and Al, namely GdAlO_3 (GAP, JCPDF No. 9-85). The orthorhombic GdAlO_3 -type perovskites ($Pbnm$), with general stoichiometry ABO_3 , are derived from the ideal cubic structure ($Pm3m$) via the tilting and distortion of the BO_6 octahedra [32]. Its framework can be regarded as a cube with a distorted oxygen octahedron at each

vertex and a Gd^{3+} ion displaced slightly within the x - y plane in the center [33]. The larger A cation is situated in the void formed by eight octahedra and, in the ideal cubic structure, this cation is surrounded by the 12 nearest neighboring oxygens at equal distances [34]. The angle of the monoclinic unit cell is $90^\circ-27'$ in this material, so twinning readily takes place during growth [35]. Gd^{3+} and Eu^{3+} have the same valence and similar ion radius ($r_{\text{Gd}^{3+}} = 0.94 \text{ \AA}$, $r_{\text{Eu}^{3+}} = 0.95 \text{ \AA}$) [36]. At 800 and 1000 °C, the XRD patterns evidence new crystalline phases that can be ascribed to $\text{Gd}_3\text{Al}_5\text{O}_{12}$ (GAG, JCPDF No. 18-517), and $\text{Gd}_4\text{Al}_2\text{O}_9$ (GAM, JCPDF No. 30-14). Also, there are phases of Al_2O_3 (JCPDF No. 2-1373) and Gd_2O_3 (Eu_2O_3). $\text{Gd}_4\text{Al}_2\text{O}_9$ (GAM) is monoclinic and its structure is related to that of the mineral cuspidine, whereas $\text{Gd}_3\text{Al}_5\text{O}_{12}$

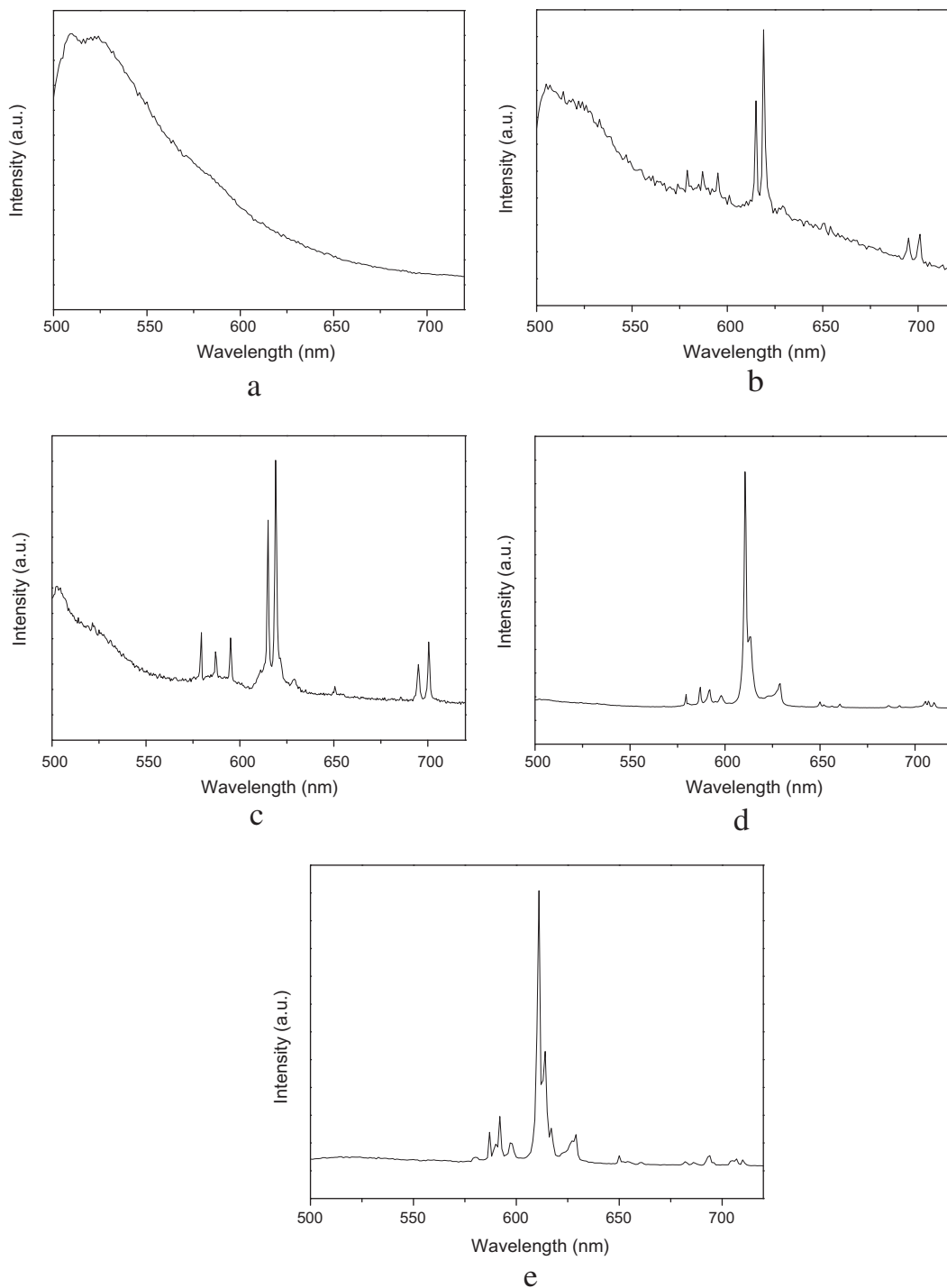


Fig. 6. Emission spectra of the Eu^{3+} ion in the $\text{Gd}(\text{Eu})\text{-Al-O}$ samples treated at (a) 100, (b) 400, (c) 600, (d) 800, and (e) 1000 °C for 4 h, excited at 467 nm ($^5\text{D}_2$ level).

(GAG) belongs to the garnet structure type [4]. Gadolinium aluminum garnet (GAG) is one of the most important phosphors host materials with cubic structure [7]. The phase transition was observed by DTA analysis.

The peaks at $2\theta = 23.05^\circ$ (GdAlO_3), 28.89° , 39.05° , 42.93° , 50.52° , and 56.06° (Gd_2O_3 or Eu_2O_3) appear in the samples treated at 400 and 600 °C. When the precursor is heated at 800 and 1000 °C, there is a new crystalline phase of the material with peaks at $2\theta = 16.96^\circ$ ($\text{Gd}_4\text{Al}_2\text{O}_9$), 20.71° , 27.16° , 30.01° , 36.11° , 54.60° , 57.63° ($\text{Gd}_3\text{Al}_5\text{O}_{12}$), 44.50° and 53.34° (Al_2O_3).

3.3. Photoluminescence (PL)

Fig. 3 depicts the excitation spectra of Eu^{3+} ion-doped $\text{Gd}(\text{Eu})\text{-Al-O}$ host samples monitored at the $^5\text{D}_0 \rightarrow ^7\text{F}_2$ transition.

The excitation spectra of the samples were recorded by fixing the emission wavelength at the Eu^{3+} : $^5\text{D}_0 \rightarrow ^7\text{F}_2$ transition. The bands can be assigned to different excitation processes. The sharp lines observed in the 350–475 nm range (f–f transitions) are attributed to transitions from the $^7\text{F}_0$ level to the $^5\text{L}_6$, $^5\text{L}_7$, and $^5\text{D}_{2-4}$ levels, for all the treated samples. The excitation spectra of the powders

Table 1

Number of bands observed for all the samples, excited at different wavelengths: CTB, 393, and 467 nm.

	$^5D_0 \rightarrow ^7F_0$ (nm)	$^5D_0 \rightarrow ^7F_1$ (nm)	$^5D_0 \rightarrow ^7F_2$ (nm)
<i>Samples $\lambda_{exc.} = CTB$</i>			
100 °C			
400 °C	579	587; 595	614; 619 ^a ; 629
600 °C	579	586; 595	614; 619 ^a ; 629
800 °C	579	586; 591; 597	610 ^a ; 614; 628
1000 °C	579	586; 589; 591; 597	610 ^a ; 614; 617; 626; 628
<i>Samples $\lambda_{exc.} = 393$ nm</i>			
100 °C	578	582; 585; 588; 592	611 ^a ; 617
400 °C	578	586; 595	614; 619 ^a ; 626; 629
600 °C	579	587; 595	610; 614; 619 ^a ; 625; 629
800 °C	579	586; 592; 598	610 ^a ; 613; 618; 629
1000 °C	579	586; 589; 591; 597	610 ^a ; 614; 616; 622; 628
<i>Samples $\lambda_{exc.} = 467$ nm</i>			
100 °C			
400 °C	579	586; 594	614; 618 ^a
600 °C	579	586; 594	610; 614; 618 ^a ; 621; 628
800 °C	579	586; 592; 594; 597	610 ^a ; 613; 622; 628
1000 °C	579	586; 589; 591; 597	610 ^a ; 613; 616; 627; 629

^a Emission maxima.

display a broad band between 250 and 330 nm, ascribed to charge transfer band (CTB) transitions in the $\text{Eu}^{3+}\text{-O}^{2-}$ bond lying in the band gap region of the Gd–Al mixed oxide host [29]. For the samples treated at 400 and 600 °C, the CTB is located at 290 nm, whereas the CTB of the materials treated at 800 and 1000 °C is located at 265 nm. The CTB energy of Eu^{3+} depends on the anion type, the binding strength of valence band electrons, and the size of the site occupied by the Eu^{3+} ions [3]. In the case of lanthanide aluminates in which the Eu^{3+} ion occupies a small site, the energy of the CTB tends to increase, so this band appears at a shorter wavelength [37]. Therefore, the symmetry of the samples treated at 800 and 1000 °C is lower than that of powders treated at 400 and 600 °C. The CTB is a measure of the covalent character of the Eu–ligand bond. The higher energy of this band indicates stronger metal–ligand interactions [38], thus the samples treated at 800 and 1000 °C have higher covalence. The sharp lines at 276, 308, and 314 nm observed in the spectra of the materials treated at 800 and 1000 °C can be attributed to energy transfer from Gd^{3+} ions to Eu^{3+} and correspond to the $^8S_{7/2} \rightarrow ^6I_{3/2}$, $^8S_{7/2} \rightarrow ^6P_J$ transitions [3,39,40].

Figs. 4–6 correspond to the emission spectra of the Eu^{3+} ion in the Gd(Eu)–Al–O host, monitored at CTB, 393 nm (5L_6 level), and 467 nm (5D_2 level), respectively.

The emission spectra of the phosphors, obtained by excitation at CTB, 393, and 467 nm, consist of $^5D_0 \rightarrow ^7F_J$ ($J=0-4$) emission lines of Eu^{3+} dominated by the $^5D_0 \rightarrow ^7F_2$ (~610 nm) electric dipole transition, which is strongly dependent on the Eu^{3+} surroundings. When the Eu^{3+} ion is situated in a low symmetry site (without inversion center), the hypersensitive transition $^5D_0 \rightarrow ^7F_2$ is often dominating in the emission spectra. This indicates that the Eu^{3+}

ion occupies a site without inversion center. The $^5D_0 \rightarrow ^7F_1$ transition (591 nm) is purely magnetic-dipole allowed, and not restricted by any symmetry [11,18].

Emission of Eu^{3+} -doped samples obtained at 100 °C present broad peaks or no peaks at all, typical of the emission profile of non-crystalline compounds or highly disordered systems (Figs. 4 and 6). In Fig. 5, the emission spectrum can be ascribed to halide precursors.

By applying the section rules for electric dipole (ED) and magnetic dipole (MD) transitions, the number of lines depends on the Eu^{3+} symmetry site, which can be determined by the allowed transitions. Usually, the splitting number of $^5D_0 \rightarrow ^7F_J$ transitions can provide information about the Eu^{3+} ions surrounding and depends on the J value and the site symmetry around Eu^{3+} , with a maximum line number of “ $2J+1$ ” for each lattice site [11,14].

A clear change in the symmetry of Eu^{3+} can be noted, since the samples present different numbers of emission lines. This indicates different symmetries for the Eu^{3+} ion. Table 1 lists the number of bands present in the emission spectra of the Eu^{3+} ion when excited at CTB, 393, and 467 nm, respectively.

The $^5D_0 \rightarrow ^7F_0$ transition appears at the same wavelength for all the samples, independent of the excitation wavelength. There is a difference concerning the relative intensity with relation to the $^5D_0 \rightarrow ^7F_1$ transition. The latter transition presents different numbers of bands, depending on the excitation wavelength and temperature. The samples treated at 400 and 600 °C display a similar number of bands, thus indicating that Eu^{3+} occupies the same symmetry site in the host, as observed by XRD. For the powders heated at 800 and 1000 °C, a new profile emission spectrum is observed. This is due to the fact that a different symmetry site is occupied by the Eu^{3+} ion, also seen in the XRD. The sample treated at 1000 °C has four peaks in the case of the $^5D_0 \rightarrow ^7F_1$ transition, more than the number allowed by $2J+1$. This is further evidence that the ion has a new surrounding.

Because Gd^{3+} and Eu^{3+} are very similar in terms of ionic radius, the doped Eu^{3+} ion occupies the Gd^{3+} sites, thereby resulting in the hypersensitive red emission transition $^5D_0 \rightarrow ^7F_2$ of Eu^{3+} , the most prominent group in the emission of this ion [13].

The emission quantum efficiency (η) of the $^5D_0 \rightarrow ^7F_2$ emission state was determined by a balance between radiative and non-radiative processes, as described in Ref. [41].

$$\eta = \tau_{\text{rad}} / (\tau_{\text{rad}} + \tau_{\text{nrad}})$$

Table 2 presents the lifetime of emissive CTB, 5L_6 , and 5D_2 to ground 5F_2 states for the samples treated at different temperatures for 4 h.

The samples excited at CTB have one lifetime only, indicating that energy transfer occurs in only one kind of Eu^{3+} site.

The biexponential decay behavior of the activator is frequently observed when the excitation energy is transferred to different Eu^{3+} sites from the donor. The samples excited at the 5L_6 and 5D_2 levels have two lifetimes, which is one more indication of the presence of different Eu^{3+} sites in the host, as demonstrated by the XRD and PL techniques.

Table 2

Lifetime (τ) of the samples containing Eu^{3+} when excited at different levels: CTB $\rightarrow ^7F_2$, $^5L_6 \rightarrow ^7F_2$ and $^5D_2 \rightarrow ^7F_2$, and quantum efficiency (%) for the samples annealed at 100, 400, 600, 800, and 1000 °C for 4 h.

	CTB $\rightarrow ^7F_2$		$^5L_6 \rightarrow ^7F_2$		$^5D_2 \rightarrow ^7F_2$		$^5D_2 \rightarrow ^7F_2$		$^5D_2 \rightarrow ^7F_2$	
	Quantum efficiency (%)		Quantum efficiency (%)		Quantum efficiency (%)		Quantum efficiency (%)		Quantum efficiency (%)	
	η_1	τ_1	η_1	η_2	τ_1	τ_2	η_1	η_2	τ_1	τ_2
100 °C	25.38	1.46	2.28	19.20	0.13	1.12	1.80	36.59	0.14	2.80
400 °C	35.75	1.25	12.36	42.79	0.38	1.30	8.93	25.29	0.49	1.39
600 °C	43.15	1.31	11.18	31.44	0.49	1.39	22.58		1.05	
800 °C	62.32	1.98	7.28	45.40	0.27	1.60	51.39		1.55	
1000 °C	55.83	2.20	39.62		1.57		5.41	43.67	0.19	1.53

In general, excitation within the f-manifold promotes high quantum efficiencies, whereas charge transfer excitation yields low efficiency. We observed one lifetime and higher quantum efficiency for the samples excited at CTB. Excitation at CTB reveals that energy transfer takes place in only one Eu^{3+} site, while the excitation in f-manifold ($^5\text{L}_6$ and $^5\text{D}_2$ levels) shows the existence of more than one Eu^{3+} site. Energy transfer to different types of site can reduce the quantum efficiency.

3.4. Infrared spectroscopy (FTIR)

The infrared spectra present the broad band at 3400 cm^{-1} represents the O–H vibrations. Its intensity decreases with rising heat treatment temperature, thus confirming the results observed by means of the TG/DTG curves. The band observed at 1630 cm^{-1} was assigned to the H–O–H band bending [42]. The samples treated at different temperatures exhibit strong bands between 400 and 800 cm^{-1} , approximately, which are typical of metal–oxygen (Gd–O and Al–O) vibrations for compounds with perovskite structure. The bands at 670 cm^{-1} can be ascribed to the Al–O (AlO_6) vibration, and those at $430\text{--}500\text{ cm}^{-1}$ correspond to Al–O (AlO_6) stretching. The band between 530 and 570 cm^{-1} can be assigned to Gd–O [3]. The other bands were not identified.

4. Conclusion

The preparation of gadolinium–aluminum oxide doped with europium by the non-hydrolytic sol–gel route has been demonstrated. Different phases such as GdAlO_3 (GAP), $\text{Gd}_3\text{Al}_5\text{O}_{12}$ (GAG), and $\text{Gd}_4\text{Al}_2\text{O}_9$ (GAM) were obtained at lower temperatures. GAP:Eu $^{3+}$ perovskite was prepared at 400 and $600\text{ }^\circ\text{C}$, while GAG and GAM doped with Eu^{3+} were obtained at 800 and $1000\text{ }^\circ\text{C}$, with mixed phases that depend on the temperature of heat treatment. FTIR analysis revealed that heat treatment at $600\text{ }^\circ\text{C}$ is sufficient to remove water molecules. The excitation spectra showed that the energy of the charge transfer bands depends on the symmetry of the Eu^{3+} ion site. The characteristic red emission of Eu^{3+} was observed in photoluminescence measurements. The lifetime and quantum efficiency depend on the excitation wavelength.

The incorporation of active species that can lead to adjustment of quantum efficiency through control of the amount of doped ions, time and treatment temperature culminates in particles with different forms and sizes, which can lead to materials with important applications as new devices.

Acknowledgements

The authors acknowledge FAPESP, CNPq, and CAPES (Brazilian research funding agencies) for support of this work.

References

- [1] A. Katelnikovas, J. Barkauskas, F. Ivanauskas, A. Beganskiene, A. Kareiva, J. Sol-Gel Sci. Technol. 41 (2007) 193.
- [2] Q. Wei, D. Chen, Opt. Laser Technol. 41 (2009) 783.
- [3] H.H.S. Oliveira, M.A. Cebim, A.A. da Silva, M.R. Davolos, J. Alloys Compd. 488 (2) (2009) 619.
- [4] S. Chaudhury, S.C. Parida, K.T. Pillai, K.D.S. Mudher, J. Solid State Chem. 180 (2007) 2393.
- [5] G. Suresh, G. Seenivasan, M.V. Krishnaiah, P.S. Murthi, J. Nucl. Mater. 249 (1997) 259.
- [6] S. Cizauskaite, V. Reichlova, G. Nenartaviciene, A. Beganskiene, J. Pinkas, A. Kareiva, Mater. Chem. Phys. 102 (2007) 105.
- [7] G.S.R. Raju, H.C. Jung, J.Y. Park, C.M. Kanamadi, B.K. Moon, J.H. Jeong, S.M. Son, J.H. Kim, J. Alloys Compd. 481 (2009) 730.
- [8] A. Sinha, A.P. Sharma, P. Gopalan, Electrochim. Acta 51 (2006) 1184.
- [9] G.S.R. Raju, J.Y. Park, H.C. Jung, B.K. Moon, J.H. Jeong, J.H. Kim, Curr. Appl. Phys. 9 (2009) e92.
- [10] E.J. Nassar, L.R. Avila, P.F.S. Pereira, C. Mello, O.J. de Lima, K.J. Ciuffi, L.C. Carlos, J. Lumin. 111 (2005) 159.
- [11] E.J. Nassar, P.F.S. Pereira, E.C.O. Nassor, L.R. Avila, K.J. Ciuffi, P.S. Calefi, J. Mater. Sci. 42 (2007) 2244.
- [12] L. Zhou, W.C.H. Choy, J. Shi, M. Gong, H. Liang, J. Alloys Compd. 463 (2008) 302.
- [13] J. Wu, B. Yan, J. Alloys Compd. 432 (2008) 293.
- [14] L. Zhou, J. Shi, M. Gong, Mater. Res. Bull. 40 (2005) 1832.
- [15] P.N.M. dos Anjos, E.C. Pereira, Y.G. Gobato, J. Alloys Compd. 391 (2005) 277.
- [16] S. Wu, S. Zhang, J. Yang, Mater. Chem. Phys. 102 (2007) 80.
- [17] B. Yang, J. Wu, Mater. Lett. 61 (2007) 4851.
- [18] L. Zhou, W.C.H. Choy, J. Shi, M. Gong, H. Liang, T.I. Yuk, J. Solid State Chem. 178 (2005) 3004.
- [19] A. Bao, C. Tao, H. Yang, J. Lumin. 126 (2007) 859.
- [20] L. Zhou, J. Shi, M. Gong, J. Rare Earths 24 (2006) 138.
- [21] J. Wu, B. Yan, J. Alloys Compd. 441 (2007) 214.
- [22] E.J. Nassar, P.F.S. Pereira, K.J. Ciuffi, P.S. Calefi, Recent Development of Luminescent Materials Prepared by the Sol–Gel Process, Nova Science Publishers Inc., 2008 (pp. 265–285, Chapter 10).
- [23] A. Cestari, L.C. Bandeira, P.S. Calefi, E.J. Nassar, K.J. Ciuffi, J. Alloys Compd. 472 (2009) 299.
- [24] P.F.S. Pereira, J.M.A. Caiut, Y. Messaddeq, S.J.L. Ribeiro, K.J. Ciuffi, L.A. Rocha, E.F. Molina, E.J. Nassar, J. Lumin. 126 (2007) 378.
- [25] K.J. Ciuffi, B.L. Caetano, L.A. Rocha, E.F. Molina, Z.N. Rocha, G. Ricci, O.J. De Lima, P.S. Calefi, E.J. Nassar, Appl. Catal. A 311 (2006) 122.
- [26] E.J. Nassar, L.R. Avila, P.F.S. Pereira, O.J. de Lima, L.A. Rocha, C. Mello, K.J. Ciuffi, Quim. Nova 28 (2) (2005) 238.
- [27] K.J. Ciuffi, O.J. de Lima, H.C. Sacco, E.J. Nassar, J. Non-Cryst. Solids 304 (2002) 126.
- [28] H. Gao, Y. Wang, J. Lumin. 122–123 (2007) 997.
- [29] M.G. Matos, P.F.S. Pereira, P.S. Calefi, K.J. Ciuffi, E.J. Nassar, J. Lumin. 129 (2009) 1120.
- [30] E.H. de Faria, A.L. Marçal, E.J. Nassar, K.J. Ciuffi, P.S. Calefi, Mater. Res. 10 (4) (2007) 413.
- [31] S. Acosta, R.J.P. Corriu, D. Leclercq, P. Lefèvre, P.H. Mutin, A. Vioux, J. Non-Cryst. Solids 170 (1994) 234.
- [32] N.L. Ross, J. Zhao, R.J. Angel, J. Solid State Chem. 177 (2004) 3768.
- [33] S.J.N. Pádua, L.A.O. Nunes, J.C. Castro, J. Lumin. 43 (1989) 379.
- [34] J.D. Bass, Phys. Earth Planet. Inter. 36 (1984) 145.
- [35] A.K. Razdan, K.K. Bamzai, V. Hangloo, P.N. Kotru, B.M. Wanklyn, J. Cryst. Growth 219 (2000) 40.
- [36] X. Gao, Y. Wang, D. Wang, B. Liu, J. Lumin. 129 (2009) 840.
- [37] P. Dorenbos, J. Lumin. 111 (2005) 89.
- [38] L.A. Souza, Y. Messaddeq, S.J.L. Ribeiro, C. Fredericci, F. Lanciotti Jr., P.S. Pzani, Quim. Nova 25 (2002) 1067.
- [39] A.A. da Silva, M.A. Cebim, M.R. Davolos, J. Lumin. 128 (2008) 1165.
- [40] L.H. Brixner, Mater. Chem. Phys. 16 (1987) 253.
- [41] D.F. Parra, H.F. Brito, J.D. Matos, L.C. Dias, J. Appl. Polym. Sci. 83 (2002) 2716.
- [42] C.-F. Chang, Y.-L. Wu, S.-S. Hou, Eng. Aspects 336 (2009) 159.